Received: 12 May 2021 | Revised: 6 October 2021 | Accepted: 12 November 2021

DOI: 10.1002/bit.28001

ARTICLE

BIOTECHNOLOGY AND BIOENGINEERING WILEY

Online estimation of changing metabolic capacities in continuous *Corynebacterium glutamicum* cultivations growing on a complex sugar mixture

Peter Sinner[1] | Marlene Stiegler[1] | Oliver Goldbeck[2] | Gerd M. Seibold[3] | Christoph Herwig[1] | Julian Kager[1,4]

[1]Research Unit of Biochemical Engineering, Institute of Chemical, Environmental and Bioscience Engineering, Technische Universität Wien, Vienna, Austria

[2]Institute of Microbiology and Biotechnology, University of Ulm, Ulm, Germany

[3]Section for Synthetic Biology, Department of Biotechnology and Biomedicine, Technical University of Denmark, Lyngby, Denmark

[4]Competence Center CHASE GmbH, Linz, Austria

Correspondence

Julian Kager, Competence Center CHASE GmbH, Ghegastraße 3, 1030 Vienna, Austria.
Email: julian.kager@chasecenter.at

Christoph Herwig, Research Unit of Biochemical Engineering, Institute of Chemical, Environmental and Bioscience Engineering Technische Universität Wien, Gumpendorferstraße 1a, 1060 Vienna, Austria.
Email: christoph.herwig@tuwien.ac.at

Funding information

COMET Center CHASE GmbH, Grant/Award Number: 868615; Novo Nordisk Fonden within the framework of the Fermentation-based Biomanufacturing Initiative, Grant/Award Number: NNF17SA0031362; German Ministry of Education and Research in the frame of the e:Bio initiative, Grant/Award Number: 555 031A302D; Bio Based Industries Joint Undertaking under the European Union's Horizon 2020 research and innovation programme, Grant/Award Number: 790507 (iFermenter)

Abstract

Model-based state estimators enable online monitoring of bioprocesses and, thereby, quantitative process understanding during running operations. During prolonged continuous bioprocesses strain physiology is affected by selection pressure. This can cause time-variable metabolic capacities that lead to a considerable model-plant mismatch reducing monitoring performance if model parameters are not adapted accordingly. Variability of metabolic capacities therefore needs to be integrated in the in silico representation of a process using model-based monitoring approaches. To enable online monitoring of multiple concentrations as well as metabolic capacities during continuous bioprocessing of spent sulfite liquor with *Corynebacterium glutamicum*, this study presents a particle filtering framework that takes account of parametric variability. Physiological parameters are continuously adapted by Bayesian inference, using noninvasive off-gas measurements. Additional information on current parameter importance is derived from time-resolved sensitivity analysis. Experimental results show that the presented framework enables accurate online monitoring of long-term culture dynamics, whereas state estimation without parameter adaption failed to quantify substrate metabolization and growth capacities under conditions of high selection pressure. Online estimated metabolic capacities are further deployed for multiobjective optimization to identify time-variable optimal operating points. Thereby, the presented monitoring system forms a basis for adaptive control during continuous bioprocessing of lignocellulosic by-product streams.

KEYWORDS

continuous bioprocessing, model adaption, nonlinear state estimation, particle filter, sensitivity analysis

1 | INTRODUCTION

Continuous bioprocessing can enable high space time yields under consistent production rates and product quality. Thereby, process intensification in comparison with regular batch or fed-batch operations is feasible. Applications of continuous microbial bioprocesses are versatile, ranging from large scale ethanol production (Sahm & Bringer-Meyer, 1987) to recent developments for recombinant protein production (Kittler et al., 2020; Schuller et al., 2020). Despite technological advantages such as reduced culture volumes and potential for continuous downstream integration (Gagnon et al., 2018), physiological instabilities still hamper the implementation of robust continuous processes (Kopp et al., 2019).

To additionally improve sustainability of biotechnological processes, lignocellulosic by-product streams such as spent sulfite liquor (SSL) can be utilized as alternative feedstocks. SSL is a complex mixture containing various hemicellulose hydrolysis products, with mannose, xylose, and glucose being the main carbohydrates accessible for bioprocessing. With quantities of around 90 billion liters of SSL being generated yearly during sulfite pulping of wood (Lawford & Rousseau, 1993) and due to its high carbohydrate content, SSL is an attractive substrate stream for industrial biotechnology. Continuous processes utilizing SSL were described for the production of various value-added-products, such as single cell protein (Gold et al., 1981), bioethanol (Mandenius, 1988; Vees et al., 2020), or succinic acid (Ladakis et al., 2018).

In this study, a recombinant *Corynebacterium glutamicum* strain is used for continuous SSL bioprocessing. *C. glutamicum* is an important industrial producer of amino acids and can be genetically modified for a wide range of potential products, including chemical building blocks (Becker et al., 2018) as well as recombinant proteins (Hemmerich et al., 2019). Strain improvements also enabled hemicellulosic sugar conversion (Buschke et al., 2013; Choi et al., 2019; Meiswinkel et al., 2013), thus making *C. glutamicum* a promising new platform for the utilization of lignocellulosic by-product streams.

Bioprocessing of by-product streams such as SSL remains challenging due to the presence of potential growth inhibitors, batch-to-batch raw material fluctuations and multiple carbon sources that can lead to reciprocal inhibition effects and therefore to substrate accumulation or inefficient utilization. During continuous processes, selection pressure on the culture introduces an additional element of complexity. Besides of process instabilities caused by the metabolic burden of recombinant gene expression (Hoffmann & Rinas, 2004; Neubauer et al., 2003; Schuller et al., 2020), the selection pressure in continuous operation can also lead to favorable biological adaptions (Wortel et al., 2016). Phenotype changes are caused by genetic (Arensdorf et al., 2002; Jansen et al., 2005; Wenger et al., 2011) and nongenetic (Herwig & von Stockar, 2002; Wright et al., 2020) adaptions and their regulatory implications have to be considered (Sato et al., 2016). Based on aforementioned effects, continuous cultivations in chemostat or turbidostat mode can be regarded as highly efficient systems for directed evolution and have therefore also been adopted for strain and protein engineering applications (Arensdorf et al., 2002; Badran & Liu, 2015; d'Oelsnitz & Ellington, 2018; Koppram et al., 2012). Long-term adaption effects that change the metabolic capacities of the culture during running processes can lead to unplanned deviations from assumed steady-state behavior. These deviations can challenge reproducibility of experiments (Wick et al., 2002) as well as stability of production processes (Kazemi Seresht et al., 2013) and limit the applicability of process models not considering parametric variability. Different models that directly simulate adaption during continuous cultivations were proposed for single carbon substrate processes (Bayen & Mairet, 2017; Koprinkova-Hristova & Patarinska, 2006; Patarinska et al., 2000; Sonnleitner & Hahnemann, 1994). However, stochastic evolution can limit the transferability of such models (Wick et al., 2002). To operate at optimal dilution rates, guaranteeing high space time yields and efficient substrate utilization, changing metabolic capacities therefore need to be monitored throughout the process.

Monitoring strategies using at-line flow cytometry (Vees et al., 2020) as well as in situ online probes, such as turbidity sensors (Gold et al., 1981), were previously applied to characterize continuous bioprocesses utilizing SSL. The use of time-consuming as well as costly at-line measurements reduces the degree of process automation and hampers targeted control actions during running operations. Online monitoring by in-line probes enables a high time resolution but in situ reactor modifications (Gold et al., 1981) or recirculation loops (Cabaneros Lopez et al., 2020a) are often necessary. Off-gas analysis offers a promising noninvasive measurement for online monitoring (Aehle et al., 2011). Online measurements can be fused with previous process knowledge in the form of dynamic models to efficiently exploit their information content. For this purpose, state observers (Ali et al., 2015) are needed and were implemented for bioprocess applications using, for example, extended Kalman filters (Narayanan et al., 2020) or particle filters (Goffaux & Vande Wouwer, 2005; Stelzer et al., 2017). Both base on Bayesian inference, whereas the particle filter approximates the probability density function by single particle simulations and the Kalman filter directly by local linearization and assumed normal distributions (Simon, 2006). Although computationally more demanding the particle filter has shown good performance for biotechnological processes (Goffaux & Vande Wouwer, 2005; Stelzer et al., 2017). In recent publications (Cabaneros Lopez et al., 2020b; Sinner et al., 2021) it was shown how model-based state estimation can be used for online monitoring during batch and fed-batch operation of lignocellulosic by-product streams. Hereby, state estimators were applied to handle different initial batch conditions or raw material uncertainties.

This study introduces state estimation for continuous bioprocesses utilizing the multisubstrate stream SSL, which are subject to elevated selection pressure. Previous state estimators for continuous stirred-tank reactors (CSTR) (diè ne Benyahia et al., 2012; Patarinska & Popova, 2003) focused on single carbon substrate processes only. Also, changes in the physiological capacity due to long-term process dynamics were not considered in these previous works. To enable state estimation of continuous processes we included potential adaption mechanisms during continuous cultures growing on SSL. To do so, simultaneous state and model parameter estimation is necessary. A straightforward approach builds on state augmentation with random walk parameter dynamics as proposed by Kitagawa (1998).

To the best of the authors' knowledge, simultaneous state and parameter estimation was previously not experimentally implemented for continuous bioprocesses subject to long-term adaption effects. The presented strategy uses off-gas measurements and is therefore noninvasive. Furthermore, estimator results are exploitable for setpoint optimization considering time-variable metabolic capacities.

The remainder of this paper is structured as follows. In Section 2 the experimental and mathematical methodologies are summarized. Obtained results for modeling and online state estimation are presented in Section 3 and discussed with a particular focus on adaption of metabolic capacities. Conclusions of the study are given in Section 4.

2 | MATERIAL AND METHODS

2.1 | Experimental set-up and cultivation conditions

Cultivation experiments were performed with a derivative of *C. glutamicum* ATCC 13032 transformed with pEKEx3-*xylAB* (Meiswinkel et al., 2013) (Spec^R, P_{trc}*lacI*^{q}, pBL1 *ori*V_{Cg}) and pVWEx1-*manA* (Schwentner et al., 2021) (Kan^R, P_{trc}*lacI*^{q}, pHM1519 *ori*V_{Cg}). Xylose utilization is enabled by pEKEx3-*xylAB*, containing the xylose isomerase gene *xylA* and the xylulokinase gene *xylB*. pVWEx1-*manA* overexpresses the mannose-6-phosphate isomerase gene *manA* for improved mannose utilization. All batch and feeding media were supplemented with antibiotics (50 µg ml^{-1} kanamycin sulfate and 100 µg ml^{-1} spectinomycin dihydrochloride). The seed train was performed as described in Sinner et al. (2021). Bioreactor processes were inoculated to reach an initial optical density at 600 nm of 8 and were conducted with working volumes of 0.2 L in a DASbox Mini Bioreactor System (Eppendorf AG) equipped with dual Rushton turbines. CGXII medium (Keilhauer et al., 1993) without urea and MOPS buffer, supplemented with 10% (v/v) ultrafiltrated SSL (UF-SSL) from softwood pulping and 1 mM IPTG, was used as batch medium. Temperature was kept at 30°C and culture pH was controlled at 6.5 by addition of 6 M ammonium hydroxide and 1 M phosphoric acid. Dissolved oxygen was controlled above 30% by a cascaded adaption of stirrer speed (400–1200 rpm) and oxygen concentration of the inlet gas (20.95% to 27.5% (v/v)) by supplementing pressurized air with pure oxygen at an overall gassing rate of 1 vvm. The chemostat phase was started when an optical density at 600 nm of 30 was reached by feeding CGXII medium without urea and MOPS buffer, supplemented with 20% (v/v) UF-SSL and 1 mM IPTG. Dilution rate setpoints in the range of 0.013–0.31 h^{-1} were applied during chemostat experiments.

2.2 | Offline analytics

For biomass dry cell weight determination, 1.8 ml culture broth were centrifuged at 10,000 rpm for 10 min at 4°C, the pellet was washed with phosphate buffered saline and was centrifuged again under identical conditions. The washed pellet was then dried in preweighed sample tubes at 105°C for 72 h before gravimetric analysis. Mannose, xylose and glucose concentrations in 0.2 µm filtrated culture supernatants were quantified by HPLC-RID using a lead column (Nucleogel Sugar Pb, Macherey Nagel). The column was operated at 80°C and deionized water was used as eluent at an isocratic flow rate of 0.4 ml min^{-1}.

2.3 | Online measurements and data analysis

Reactor parameters, gas and liquid inflow rates were retrieved online from the DASbox reactor system using the DASware control software (Eppendorf AG) (see Figure 1). CO_2 and O_2 off-gas concentrations were measured online using a DASGIP GA4 gas analyzer (Eppendorf AG) based on galvanic cells for O_2 and infrared sensor modules for CO_2 determination. Online data transfer between the DASware control software and the numerical computing environment Matlab R2020a (The MathWorks, Inc.) was enabled by OPC DA. All subsequent data analysis was conducted in Matlab running on a conventional work station (Intel Core i5-4670U CPU 3.40 GHz, 16 GB RAM). Using online off-gas concentration measurements and inflow of air and pure oxygen, carbon dioxide evolution (CER) and oxygen uptake (OUR) rates were calculated according to Aehle et al. (2011). Hereby, an equilibrium between liquid and gaseous phase was assumed for constant pH and temperature during controlled bioreactor conditions (Aehle et al., 2011; Spérandio & Paul, 1997). Biomass specific growth and substrate uptake rates were derived from the offline analytics (Section 2.2) by solving the mass balance assuming a constant rate between two sampling time points as described by Kroll et al. (2017).

2.4 | Nonlinear process model

The CSTR process model describes mass concentration balances of biomass X, glucose S_1, mannose S_2 and xylose S_3 states (g L^{-1}) in the ordinary differential equation (ODE) system shown in Equation (1). The model builds on previous work of Sinner et al. (2021) and is extended with maintenance coefficents m_{Si}, which are especially relevant at low dilution rates.

$$\begin{pmatrix}\dot{S}_1\\ \dot{S}_2\\ \dot{S}_3\\ \dot{X}\end{pmatrix} = \begin{pmatrix}-\left(\frac{1}{Y_{XS1}}+\frac{m_{S1}}{\mu_{S1}}\right) & 0 & 0\\ 0 & -\left(\frac{1}{Y_{XS2}}+\frac{m_{S2}}{\mu_{S2}}\right) & 0\\ 0 & 0 & -\left(\frac{1}{Y_{XS3}}+\frac{m_{S3}}{\mu_{S3}}\right)\\ 1 & 1 & 1\end{pmatrix}\begin{pmatrix}\mu_{S1}\\ \mu_{S2}\\ \mu_{S3}\end{pmatrix}X + \frac{\dot{V}_R}{V_R}\begin{pmatrix}S_{1\,in}-S_1\\ S_{2\,in}-S_2\\ S_{3\,in}-S_3\\ -X\end{pmatrix} \quad (1)$$

V_R represents the reactor volume (L) and $\dot{V}_R$ (L h^{-1}) the volumetric flow rate giving the current dilution rate D (h^{-1}) as $D = \dot{V}_R/V_R$. The respective carbon substrate concentrations (g L^{-1}) in the feed

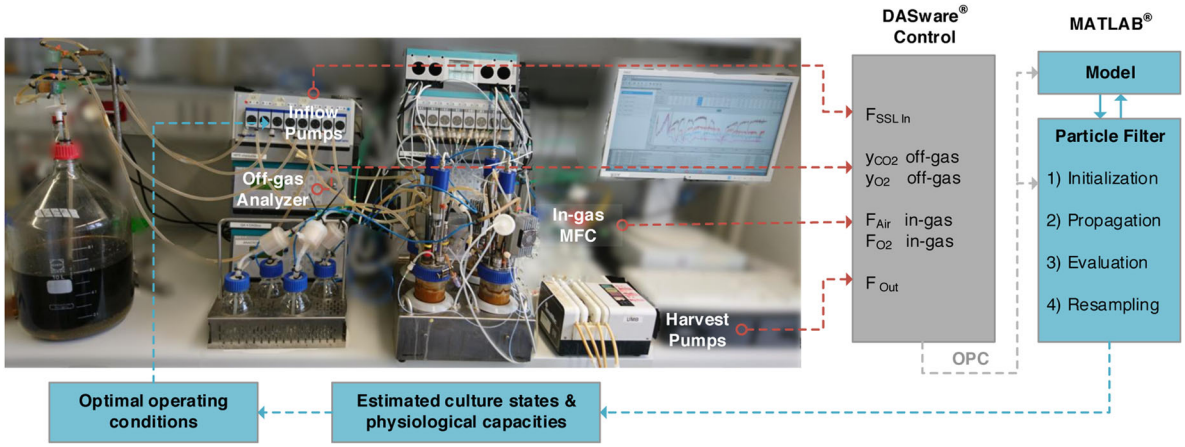

FIGURE 1 Experimental setup using a DASbox reactor system (Eppendorf AG). The measurements needed for particle filtering were transferred to MATLAB by OPC (Open Platform Communication). Based on the resulting estimated states and metabolic capacities the current optimal operating conditions can be re-evaluated

medium are denoted by $S_{i\ in}$. Biomass yield coefficients Y_{XSi}, specific growth rates μ_{Si}, and substrate specific maintenance coefficients m_{Si} couple biomass formation with substrate consumption q_{Si}. The kinetics of biomass growth are described in Equations (2)–(4), including competitive substrate inhibition effects by glucose adapted from Yoon et al. (1977) and Sinner et al. (2021). Hereby, $\mu_{max\ Si}$ denotes the biomass specific maximum growth rate on substrate S_i and K_{Si} the respective substrate affinity coefficient. The biomass specific maximum substrate uptake rates for biomass formation can be derived as $q_{max\ Si} = \mu_{max\ Si}/Y_{XSi}$.

$$\mu_{S1} = \mu_{max\ S1}\frac{S_1}{S_1 + K_{S1}} - m_{S1}Y_{XS1} \tag{2}$$

$$\mu_{S2} = \mu_{max\ S2}\frac{S_2}{S_2 + \frac{K_{S2}}{K_{S1}}S_1 + K_{S2}} - m_{S2}Y_{XS2} \tag{3}$$

$$\mu_{S3} = \mu_{max\ S3}\frac{S_3}{S_3 + \frac{K_{S3}}{K_{S1}}S_1 + K_{S3}} - m_{S3}Y_{XS3} \tag{4}$$

Model parametrization was performed on training data using identifiable parameter subsets (Brun et al., 2001; Ulonska et al., 2018). Model parameters (θ), including estimated parameters and model constants, are given in Table 1. Uncertainties of model simulations were derived by 100 Monte Carlo simulations with uniform random sampling from $\theta \pm 3\sigma$, using parameter uncertainties σ obtained from the inverse Fisher information matrix.

Carbon dioxide evolution (CER) and oxygen uptake (OUR) rates (mol h^{-1}) were modeled by carbon and redox balancing, see Equations (5) and (6), as described previously using a measured elemental composition of *C. glutamicum* growing on SSL (Sinner et al., 2021). Carbon balancing is hereby based on biomass formation and sugar consumption using the weight of a respective sugar compound per mole of carbon contained, $M_{C\text{-}mol\ Si}$, and the weight per mole of carbon of biomass, $M_{C\text{-}mol\ X}$. Redox balancing is based on the degree of reduction (Minkevich & Eroshin, 1973) of biomass DOR_X, the respective degree of reduction of the main carbon substrates glucose, mannose and xylose DOR_{Si} and the degree of reduction of oxygen DOR_{O_2}. Degrees of reduction of organic compounds are obtained as the number of equivalents of electrons per C-mol that are available upon oxidation. The degree of reduction of an element within a compound hereby corresponds to the valence of this element (C = 4, H = 1, N = −3, O = −2, P = 5, S = 6). For oxygen O_2 as an electron acceptor. Parameters used for modeling are listed in Table 1. As outlined in Section 2.3 an equilibrium between liquid and gaseous phase can be assumed under constant pH and temperature conditions. This allows for a simplified simulation of gas phase dynamics, where an additional consideration of CO_2 hold-up in the liquid phase can be omitted.

$$CER = XV_R\sum_{i=1}^{3} q_{Si}\left(\frac{1}{M_{C\text{-}mol\ Si}} - \frac{Y_{XSi}}{M_{C\text{-}mol\ X}}\right) \tag{5}$$

$$OUR = \frac{XV_R}{DOR_{O_2}}\sum_{i=1}^{3} q_{Si}\left(\frac{DOR_{Si}}{M_{C\text{-}mol\ Si}} - \frac{Y_{XSi}\ DOR_X}{M_{C\text{-}mol\ X}}\right) \tag{6}$$

2.5 | Particle filter algorithm for simultaneous state and parameter estimation

For online state estimation, the ODE system of Equation (1) is presented as the system model in the general form of Equation (7). Hereby, the time derivative $\dot{x}$ of process states $x = (X, S_1, S_2, S_3)$ is a function f of the current states x, the dynamic inputs u ($D = \dot{V}_R/V_R$) and the model parameters and constants θ. To integrate the online off-gas measurements $y = (CER, OUR)$ for state estimation, a measurement model, Equation (8), is defined as a function h of the current states x and the model constants θ based on carbon and electron balances described in Equations (5) and (6).

$$\dot{x} = f(t, x, u, \theta) \tag{7}$$

$$y = h(x, \theta) \tag{8}$$

TABLE 1 Model parameters of the *C. glutamicum* chemostat process model

Parameter	Value	Standard deviation	Unit	Source
$S_{1\,in}$	7.81	–	g L^{-1}	Measured
$S_{2\,in}$	23.96	–	g L^{-1}	Measured
$S_{3\,in}$	10.38	–	g L^{-1}	Measured
$M_{Cmol\ S_{1,2,3}}$	30.03	–	g $Cmol^{-1}$	Calculated
$M_{Cmol\ X}$	27.78	–	g $Cmol^{-1}$	Sinner et al. (2021)
DOR_{O_2}	−4.00	–	mol_{e^-} $Cmol^{-1}$	Calculated
$DOR_{S_{1,2,3}}$	+4.00	–	mol_{e^-} $Cmol^{-1}$	Calculated
DOR_X	+4.18	–	mol_{e^-} $Cmol^{-1}$	Sinner et al. (2021)
Y_{XS1}	0.576	±0.010	g g^{-1}	Parameter estimation
Y_{XS2}	0.596	±0.011	g g^{-1}	Parameter estimation
Y_{XS3}	0.545	±0.024	g g^{-1}	Parameter estimation
$\mu_{max\ S1}$	0.140	±0.004	h^{-1}	Parameter estimation
$\mu_{max\ S2}$	0.074	±0.001	h^{-1}	Parameter estimation
$\mu_{max\ S3}$	0.049	±0.001	h^{-1}	Parameter estimation
K_{S1}	2.2×10^{-3}	$\pm 0.23 \times 10^{-3}$	g L^{-1}	Parameter estimation
K_{S2}	0.094	±0.019	g L^{-1}	Parameter estimation
K_{S3}	0.046	±0.019	g L^{-1}	Parameter estimation
m_{S1}	4.3×10^{-3}	$\pm 0.12 \times 10^{-3}$	g g^{-1} h^{-1}	Parameter estimation
m_{S2}	0.011	$\pm 0.14 \times 10^{-3}$	g g^{-1} h^{-1}	Parameter estimation
m_{S3}	3.8×10^{-3}	$\pm 0.13 \times 10^{-3}$	g g^{-1} h^{-1}	Parameter estimation

The system model, Equation (7), and measurement model, Equation (8), were integrated in a bootstrap particle filter. The particle filter implementation is based on Gordon et al. (1993) and Simon (2006). It constitutes a sequential Monte Carlo algorithm that uses Bayesian interference to reconstruct the most likely current process states $x$based on the measurments y.

For initialization, a random sample of $N = 500$ particles $\{x_0^i : i = 1, \ldots, N\}$ is drawn from the assumed probability density function (pdf) $p(x_0)$ at initial time point $k = 0$. To enable joint estimation of process states x and parameters θ, the state space is augmented with a parameter vector (Kitagawa, 1998). Gaussian random walk with parameter noise variance $\xi = 0.1 \cdot \theta_{a,0}$ is used to add artificial dynamics to the most sensitive subset (parameter importance ranking shown in Appendices) of kinetic parameters $\theta_a = (\mu_{max\ S1}, \mu_{max\ S2}, \mu_{max\ S3})$. Hereby 0.1 is a noise tuning factor, which is in the range of typical model parameter uncertainties as reported by Brun et al. (2001). This parameter perturbation, Equation (9), represents phenotypic plasticity during chemostat operation and is performed iteratively for each time step $k \geq 1$ (calculation interval 40 min) by using the normally distributed perturbation vector $p_k^i \sim \mathcal{N}(0, \xi)$. Hereby, the parameter values estimated in the previous time step, $\hat{\theta}_{a,k-1}$, are used.

$$\theta_{a,k}^i = \hat{\theta}_{a,k-1} + p_k^i \quad (i = 1, \ldots, N) \tag{9}$$

Using the changed parameter values $\theta_{a,k}^i$ within system model equations f, a priori particles $\tilde{x}_k^i$ (process states) are propagated under addition of process noise w_{k-1}^i at each time step $k \geq 1$, Equation (10). Process noise levels of $\Sigma_{wk} = \mathrm{diag}\left(\sigma_X^2, \sigma_{S_1}^2, \sigma_{S_2}^2, \sigma_{S_3}^2\right) = \mathrm{diag}(4.9 \times 10^{-5}, 1 \times 10^{-10}, 2.5 \times 10^{-5}, 4 \times 10^{-6})$ were applied as reported previously (Sinner et al., 2021).

$$\tilde{x}_k^i = f(x_{k-1}^i) + w_{k-1}^i \quad (i = 1, \ldots, N) \tag{10}$$

The augmented state vector is denoted as $z_k^i = \left\{x_k^i, \theta_{a,k}^i\right\}$ in the following. Based on available online measurements y^*, measurement variance matrix R and measurement model function h the relative likelihood $\tilde{q}_k^i$ is evaluated for each particle in Equation (11) (Simon, 2006). If one measurement type is currently out of specification limits, for example, during temporary technical malfunction, the estimator only considers the remaining measurement signals.

$$\tilde{q}_k^i = p(y^*|\tilde{z}_k^i) \sim \frac{1}{2\pi^{m/2}|R|^{1/2}} exp\left(\frac{-\left[y^* - h\left(\tilde{z}_k^i\right)\right]^T R^{-1}\left[y^* - h\left(\tilde{z}_k^i\right)\right]}{2}\right) \quad (11)$$

The relative likelihoods are then normalized (Simon, 2006):

$$q_k^i = \frac{\tilde{q}_k^i}{\sum_{j=1}^{N} \tilde{q}_k^j} \quad (12)$$

Subsequently, multinomial resampling from $\tilde{z}_k^i$ gives a posteriori particles z_k^i. The obtained particles z_k^i are distributed according to the desired pdf $p(z_k|y_k)$. Particle means $\bar{z}_k$ are the most likely estimation outputs for the current process states $\hat{x}_k = (X, S_1, S_2, S_3)$ and the evolved parameters $\hat{\theta}_{a,k} = (\mu_{max\ Si})$. Online biomass specific growth and substrate uptake rates are derived from the a posteriori particles. To assess estimator accuracy, the root mean square error (RMSE) between offline measured and online estimated states was calculated. Normalization by the range of offline measured states in the given data set gives the normalized root mean square error ($NRMSE_{max\text{-}min}$).

2.6 | Online parametric sensitivity analysis

Parametric sensitivity analysis was performed locally at each calculation time point of the state estimator (Section 2.5). Sensitivity of the kinetic model parameters $\theta_a = (\mu_{max\ Si})$ regarding different process states can be analyzed. Within this system, the local parametric sensitivities on the measured outputs CER and OUR (Equations 5 and 6) were determined. As only low and steady parameter changes are expected a local analysis can be regarded as satisfactory for this application. First-order partial derivatives of measurement model $h(x, \theta)$ with respect to kinetic parameters θ_a give the sensitivity matrix S_k ($m \times n$, for m process states and n kinetic parameters) at time step k using the latest state estimates $\hat{x}_k$ and parameter estimates $\hat{\theta}_{a,k}$:

$$S_k = \left.\frac{\partial h(x, \theta_a)}{\partial \theta_a}\right|_{\substack{x=\hat{x}_k \\ \theta_a=\hat{\theta}_{a,k}}} \quad (13)$$

The elements $s_{m,n}$ of sensitivity matrix S_k were normalized with the latest parameter estimate $\hat{\theta}_{a,k,n}$ and online measurement value y_m^*.

$$s_{norm\ m,n} = s_{m,n} \frac{\hat{\theta}_{a,k,n}}{y_m^*} \quad (14)$$

The absolute values of the rows of the resulting normalized sensitivity matrix $S_{norm,k}$ were then summed up to conjoin the sensitivities regarding the m different process states (here $m = 2$ for CER and OUR) at time point k. This gives the sensitivity vector $s_{sum,k}$.

$$s_{sum,k} = \sum_{i=1}^{m} |S_{norm,k\ m}| \quad (15)$$

2.7 | Multiobjective optimization

To analyze the process behavior of the chemostat for variable metabolic capacities, multiobjective optimization was performed using a controlled, elitist genetic algorithm (*gamultiobj*, Matlab R2020a, population size 50, Pareto fraction 0.35, stall generation limit 100, generation limit 1000) based on NSGA-II (Deb et al., 2002). Dilution rate D was varied as process parameter (0.001 h^{-1} lower bound, 0.4 h^{-1} upper bound) to obtain Pareto-optimal solutions maximizing volumetric productivity for biomass (Objective 1) and minimizing metabolizable sugar loss in the effluent (Objective 2). Online parameter estimates (Section 2.5) obtained after different process times were hereby used. Objective functions were scaled with the maximum volumetric biomass productivity $STY_{max,\hat{\theta}\ t=0}$ for the initial parameter set $\hat{\theta}_{t=0}$ and the substrate concentrations $S_{i\ in}$ in the feed medium:

$$\min_D 1 - \frac{X_{steady\ state} D}{STY_{max,\hat{\theta}\ t=0}} \quad (16)$$

$$\min_D \frac{\sum_{i=1}^{3} S_{i\ steady\ state}}{\sum_{i=1}^{3} S_{i\ in}} \quad (17)$$

3 | RESULTS AND DISCUSSION

3.1 | Dynamic model for SSL utilization in continuous operation

As a basis for model-based process monitoring, the SSL utilization kinetics of *C. glutamicum* were characterized using chemostat training data including an initial batch process phase and transient behavior upon dilution rate changes (Figure 2). Dilution rate in the chemostat phase was kept at 0.043 h^{-1} with a short phase (10 h, 3.7 residence times) with higher dilution rate of 0.27 h^{-1} at about 230 h process time. This short increase resulted in an accumulation of unmetabolized substrate in the effluent stream and washout of biomass before the system returned to steady state operation at low dilution rate.

The kinetic process model described in Section 2.4 was parameterized on this training data set and the obtained model parameters are shown in Table 1. Low parametric uncertainty with coefficients of variation below 5% for all parameters besides of xylose affinity coefficient (42%) was observed. Comparing experimental and simulated target states, low root mean square errors (RMSE) for biomass (1.7 g L^{-1}), glucose (0.31 g L^{-1}), mannose (1.6 g L^{-1}), xylose (0.37 g L^{-1}) as well as CER (0.0016 mol h^{-1}) and OUR (0.0016 mol h^{-1}) states were achieved. This corresponds to normalized root mean square errors (NRMSE) below the acceptance criterion of 15% (Ulonska et al., 2018) for all target states of sugar uptake and biomass formation for *C. glutamicum* utilizing SSL in a continuous bioprocess.

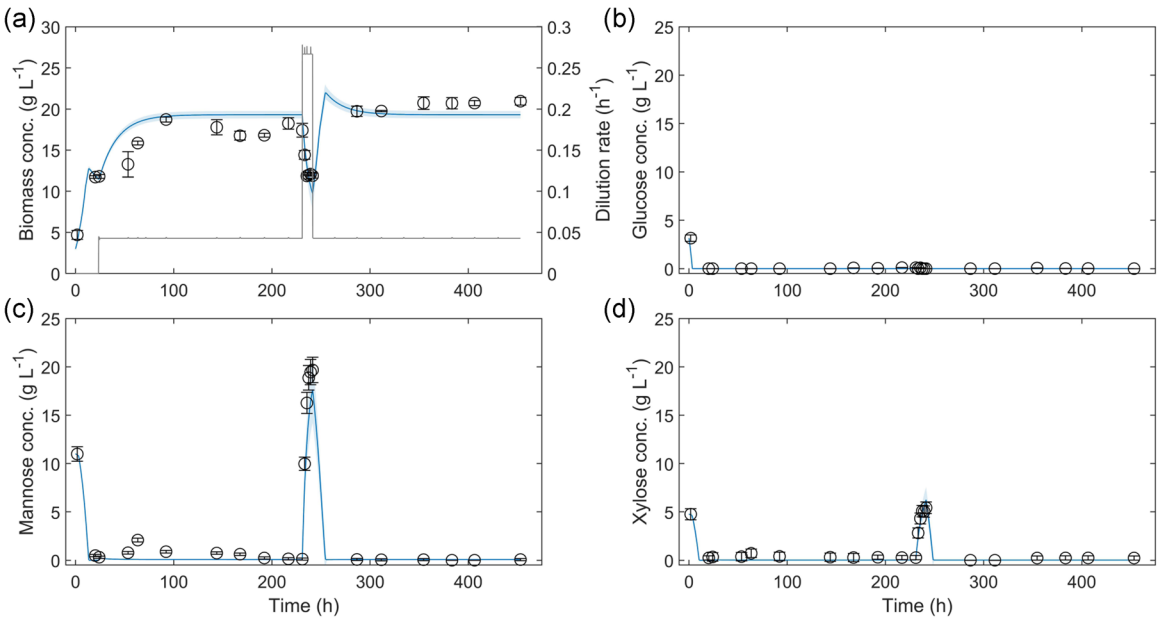

FIGURE 2 Measured (black, circles) and simulated (blue, lines) concentrations of (a) biomass (1.7 g L^{-1} RMSE model error), (b) glucose (0.31 g L^{-1} RMSE model error), (c) mannose (1.6 g L^{-1} RMSE model error) and (d) xylose (0.40 g L^{-1} RMSE model error) for chemostat training data (Data set 1). The applied dilution rates (grey, line) are shown in (a). Error bars and shaded areas indicate 95% confidence intervals. RMSE, root mean square error

TABLE 2 Overview of used data sets and corresponding estimation errors for biomass, glucose, mannose, and xylose (RMSE and $NRMSE_{max\text{-}min}$) as well as critical dilution rates (D_{crit})

		Usage		Estimation error RMSE [g L^{-1}] (NRMSE [%])				Estimated D_{crit}
Data set	Dilution rate D [h^{-1}]	Calibration	Validation	Biomass	Glucose	Mannose	Xylose	[h^{-1}]
1	0.043 (spike with 0.27)	•		1.7[a] (10.6)	0.31[a] (9.6)	1.6[a] (8.4)	0.37[a] (6.7)	0.23[a] (const)
2	0.024		•	0.71[b] (32.3)	0.020[b] (46.2)	0.27[b] (47.3)	0.20[b] (56.5)	0.23[b] (const)
3	0.077–0.31		•	6.1[b] (46.7)	1. 8[b] (1090.1)	7. 9[b] (47.9)	1. 0[b] (9.6)	0.23[b] (const)
3	0.077–0.31		•	1.4[c] (10.3)	0.037[c] (23.1)	0.73[c] (4.4)	1. 5[c] (14.0)	0.23–0.32[c]

[a]Model calibration.

[b]Standard state estimation with constant model parameters.

[c]State estimation with model parameter adaption.

Although a high dilution rate corresponds to an elevated selection pressure with potential adaption effects, the resulting model with constant parameters, such as maximum substrate specific growth rates and substrate affinities over time, did not indicate changing metabolic capacities after the short phase of high dilution rate in the training data set. As the process dynamics including the batch startup phase and the transient behavior between different dilution rates are well described by the model, it can be used as basis for online state estimation.

3.2 | Online state estimation assuming constant metabolic capacities

The parameterized model (see Section 2.4 Equations 1–4 and Table 1) was used for online state estimation under usage of a particle filter algorithm (see Section 2.5) including noninvasive off-gas analysis as online measurements. The state estimator was applied on two *C. glutamicum* chemostat processes (Table 2). One process was operated at a constant low dilution rate of 0.024 h^{-1} (Data set 2) whereas the second process was run with stepwise increasing dilution rates in the range of 0.077 to 0.31 h^{-1} (Data set 3). For the assumption of constant metabolic capacities over time model parameter adaption was turned off ($\xi = 0.0 \times \theta_{a,0}$), resulting in a standard particle filter that only incorporates process and measurement noise.

Based on the alignment of the model outputs of the propagated particels to the off-gas measurements, state estimates of biomass, glucose, mannose, and xylose concentrations of Data set 2 & 3 (blue line, Figures 3 and 4) were derived by Bayesian inference. The alignment between off-gas measurements (black line) and filtered model outputs (blue line) is displayed in Figure 5. With RMSE errors for biomass concentration below 0.71 g L^{-1} and below 0.27 g L^{-1} for

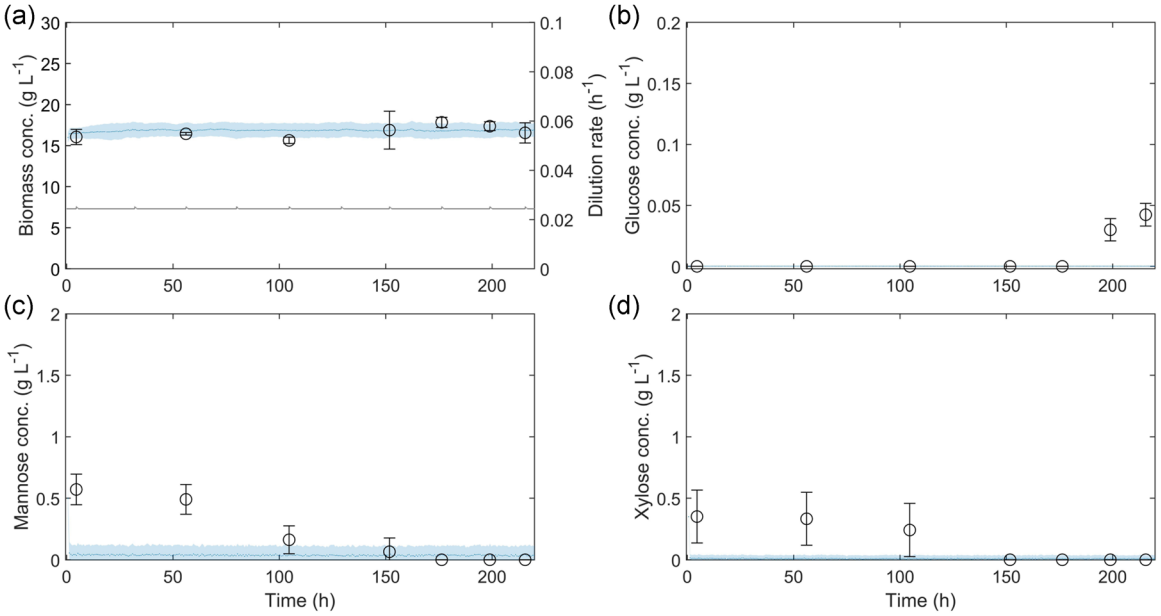

FIGURE 3 Online monitoring performance during validation chemostat run (Data set 2) with dilution rate (a) of 0.024 h^{-1} (grey, line). Offline measured validation data (black, circles) and online estimated (a) biomass, (b) glucose, (c) mannose and (d) xylose concentrations are shown for particle filtering with constant metabolic capacity (blue, dotted line). Error bars and shaded areas indicate 95% confidence intervals

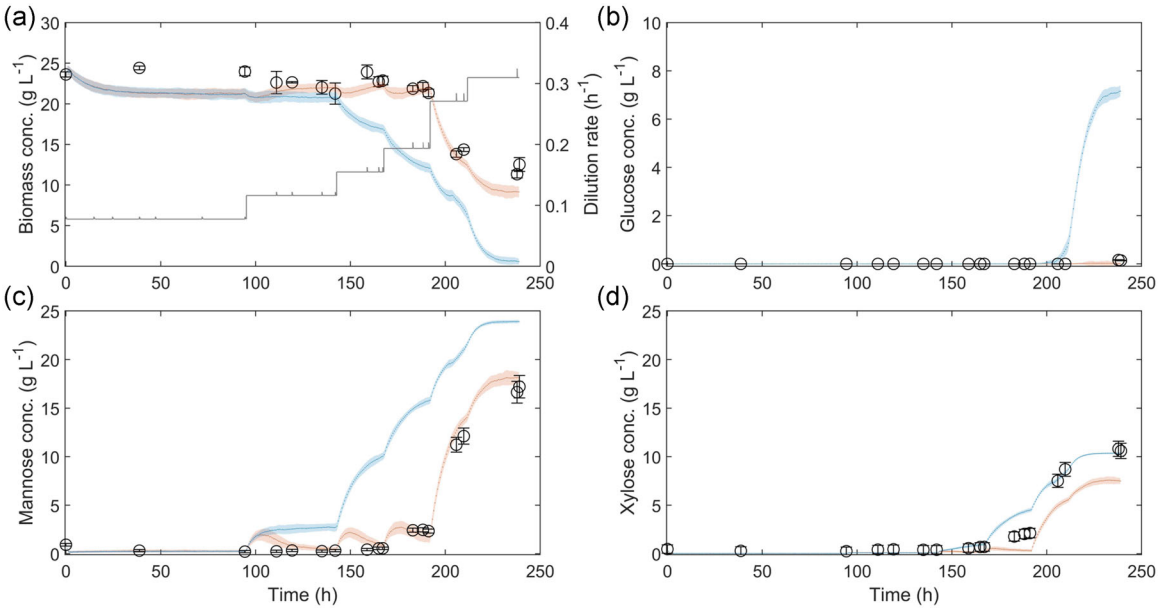

FIGURE 4 Online monitoring performance during chemostat run (Data set 3) with increasing dilution rates (a) (grey, line). Offline measured validation data (black, circles) and online estimated (a) biomass, (b) glucose, (c) mannose, and (d) xylose concentrations are shown for particle filtering with constant metabolic capacity (blue, dotted line) and with parameter adaption (orange, dotted line). Error bars and shaded areas indicate 95% confidence intervals

glucose, mannose, and xylose substrate states, accurate online state estimation was achieved for Data set 2 without the need of any additional at-line analytics. The filter was also applied to the second validation process (Data set 3) with a stepwise increase of dilution rates and thus selection pressure. The results are displayed with a blue line in Figure 4. When applying this conventional particle filter with constant metabolic capacities (no model parameter adaption), the process behavior is only inadequately estimated (blue line, Figure 4).

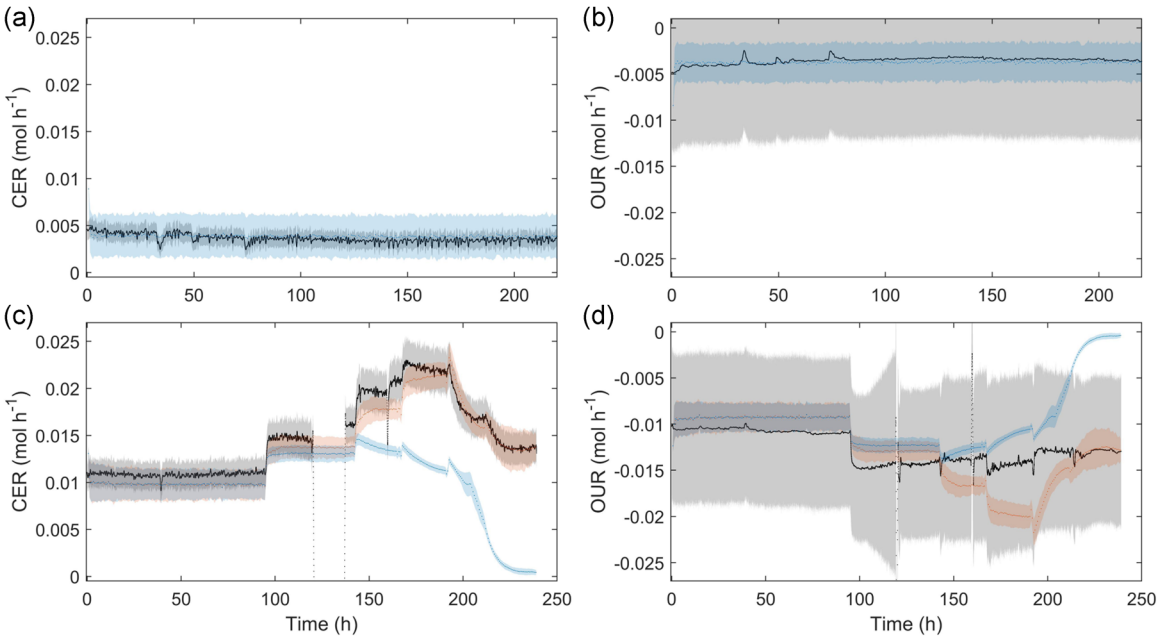

FIGURE 5 Alignment of online measurements (black, dotted line) and corresponding filtered measurement estimates using a particle filter algorithm with constant (blue, dotted line) or adapted model parameters (orange, dotted line). (a) Carbon dioxide evolution rate (CER) and (b) oxygen uptake rate (OUR) dynamics during a chemostat validation run with constant dilution rate (Data set 2). (c) CER and (d) OUR dynamics during a chemostat validation run with increasing dilution rate setpoints (Data set 3). Shaded areas indicate 95% confidence intervals. During temporary CO_2 sensor malfunction only the remaining OUR signal is considered during filtering (between 120 and 137 h)

This is also reflected in the insufficient alignment of off-gas measurements and filtered model outputs (blue line, Figure 5). During late process phases with increased dilution rates, an approach to washout equilibrium is wrongly predicted by the state estimator, leading to highly inaccurate biomass and substrate estimates. The wrongly estimated accumulation of glucose, starting from app. 200 h process time, leads to strong (simulated) reciprocal substrate uptake inhibition effects and therefore to an increasing deviation between online estimated and actual culture behavior. High RMSE errors above 6.1 g L^{-1} for biomass, 1.8 g L^{-1} for glucose and 7.9 g L^{-1} for mannose concentrations are therefore obtained.

Although a standard particle filter implementation based on Simon (2006) could be transferred from a recently published fed-batch application (Sinner et al., 2021) to a continuous process mode, a model and filter using static parameters can show limited applicability. This is especially relevant for prolonged continuous processes subject to high selection pressure due to high or increasing dilution rates over time.

Since the model includes reciprocal sugar interaction a slight change in uptake capacities and affinities, reflected in the model parameters $\mu_{max\ Si}$ and K_{Si}, greatly affects the process behavior at higher dilution rates. Under these conditions, a small overestimation of equilibrium substrate concentrations strongly influences overall growth. A standard state estimator using constant model parameters can therefore underestimate metabolic capacities and thus the current optimal dilution rate. This will lead to CSTR operation in suboptimal regions.

3.3 | Online state estimation with adaptive metabolic capacities

To include state and parametric uncertainty a particle filter was used as described in Section 2.5. Hereby, selected model parameters were integrated by state augmentation. Model parameters were adapted with with random walk dynamics ($\xi = 0.1 \times \theta_{a,0}$) in the particle propagation step. To prevent collinear behavior, for example, within the Monod terms, only the kinetic parameters $\mu_{max\ Si}$ were selected as adaptive, while all other model parameters (see Table 1) were assumed to be constant. The aim of the presented online monitoring system is the accurate estimation of process states and overall metabolic capacities with relevance for process engineering. In case online reidentification of the entire parameter set is targeted, additional measurements must be included to ensure identifiability. An identifiability analysis of the model is shown in the supplementary file.

The estimation results of the particle filter with model parameter adaption are shown in Figure 4 (orange line). For the region with lower dilution rate (0.077 h^{-1}) until about 100 h process time both filtering strategies (blue line for constant metabolic capacity, orange line for adaptive metabolic capacities) show similar performance. During the phase of stepwise increasing dilution rates the different filter behaviors can be clearly seen when comparing the off-gas measurement alignments (blue vs. orange line, Figure 5c,d). Whereas the particle filter with constant model parameters fails, the adaptive filter enables accurate online monitoring of concentration states

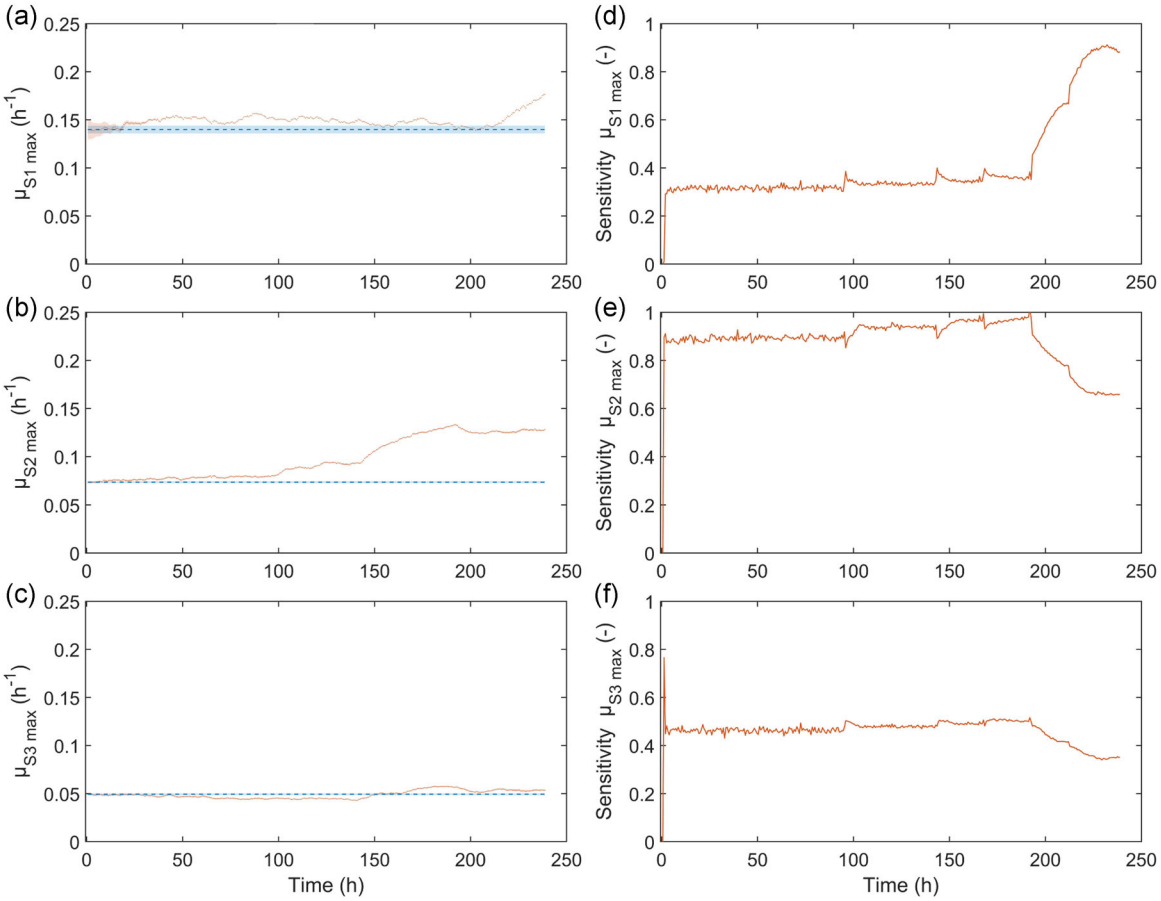

FIGURE 6 Online parameter adaption and parametric sensitivity analysis. Maximum specific growth rates on (a) glucose, (b) mannose, and (c) xylose are shown for a particle filter with constant model parameters (blue, dashed lines) or parallel state and parameter estimation (orange, solid lines). Blue shaded areas indicate 95% confidence intervals of model parameters as obtained from calibration Data set 1. Online local sensitivities (normalized) of maximum specific growth rate parameters for (d) glucose, (e) mannose, or (f) xylose utilization are shown as a measure for current selection pressure regarding the respective carbon substrate

throughout the entire CSTR process. Using the particle filter with parameter adaption (see Figure 4), estimation accuracy (RMSE) of concentration states (see Table 2) was improved by 77% for biomass, 98% for glucose and 91% for mannose in comparison to a particle filter with constant model parameters. Estimation accuracy of xylose, the substrate of lowest importance for the given process (see Section 3.4), was reduced by 50%. Low RMSE errors on biomass of 1.4 g L^{-1} and below 1.6 g L^{-1} for the substrates were achieved. This demonstrates that a particle filter with model parameter adaption is capable to monitor long-term chemostat dynamics under conditions of increasing selection pressure during utilization of SSL with *C. glutamicum*. With a runtime of 2 min 30 s for every calculation step the algorithm can be run on conventional work stations (see Section 2.3) and necessary gas analytics can be integrated in the exhaust gas stream of a CSTR without the need of reactor modifications for in situ sensor placement. The time-resolved behavior of adapted model parameters and its physiological relevance is outlined in the following section.

3.4 | Online sensitivity analysis to gain insights into selection pressure and potential physiological adaption

The maximum growth capacities on the three main sugars ($\mu_{max\ Si}$ on glucose, mannose, and xylose) are shown in Figure 6 over time. The dotted line displays constant model parameters as derived from model parametrization on calibration data (Data set 1) whereas the solid line displays the online adapted parameters during the second validation process (Data set 3). These maximum growth rates constitute kinetic model parameters and can be directly linked to the uptake capacities via the biomass to substrate conversion coefficients (Y_{XSi}) of three sugars. In addition, the respective time-resolved sensitivities of the three parameters on the measured gas conversion rates (CER and OUR) are displayed in Figure 6.

From the estimated parameter trajectory it can be seen that mainly utilization capacities for mannose (74% increase) and also for glucose (26% increase) improved, whereas xylose uptake remained

largely unaffected (8% increase). Changes of selection pressure on utilization capacity of the respective substrates can be quantified by the parametric sensitivities, which show a process phase-dependent behavior. The capacity for growth on mannose, being the main carbon substrate consumed in the SSL sugar mixture, shows highest overall sensitivities and is therefore the first to be adapted. At very high dilution rates towards the end of the process, glucose inflow approaches the current consumption capacity. Commencing glucose accumulation leads to reciprocal sugar inhibition in the given macroscopic kinetic model and thereby leads to an increased selection pressure regarding glucose consumption resulting in the increase of $\mu_{max\ S1}$ (Figure 6 from 200 h onward). Increased relevance of transcriptional control was identified previously under glucose-rich growth conditions (Graf et al., 2020) and may underlie the culture behavior observed at elevated dilution rates with substrate accumulation.

As xylose is not a native substrate for *C. glutamicum*, the pathway for xylose metabolization was artificially added by heterologous expression of *xylA* and *xylB* (Meiswinkel et al., 2013) and therefore lacking natural regulatory mechanisms. Xylose is taken up via the myo-inositol/proton symporter IolT1. The transporter gene is constitutively expressed in glucose-limited chemostat cultivation and reduced expression was observed under glucose-rich conditions (Graf et al., 2020). Expression is however not directly linked to xylose availability, indicating that it is not one of its natural substrates (Brüsseler et al., 2018). Also, xylose has been described to show poor performance as carbon source (Buschke et al., 2013) and can therefore be regarded as a minor target for adaption effects. While glucose and mannose have their entry point in glycolysis, xylose directly enters the non-oxidative part of the pentose phosphate pathway (PPP). Accordingly, cells cultivated on xylose alone show a high flux through the non-oxidative part of the PPP and need to compensate the lower NADPH output from the oxidative PPP with a higher flux through the TCA cycle (Buschke et al., 2013). Although mannose consumption can be increased by overexpression of the mannose-6-phosphate isomerase gene *manA*, strains still show a clear preference for glucose (Sasaki et al., 2011). Glucose uptake in *C. glutamicum* is mainly catalyzed by the glucose specific phosphoenolpyruvate:sugar phosphotransferase system (PTS) PtsG and to a lesser extent via the IolT1 and IolT2 symporters (Lindner et al., 2011). Mannose, an epimer of glucose, is also transported by PtsG but can also be taken up with less efficiency via the fructose-specific PtsF (Sasaki et al., 2011). Hence, both mannose and xylose compete for their major uptake system with glucose, i.e. PtsG and IolT1, which is also reflected in the process model structure, see Eqs. (3) and (4). Given a higher affinity of these transporters to glucose, as previously described for glucose and glucosamin uptake via PtsG (Uhde et al., 2013), higher extracellular glucose availability negatively affects uptake of mannose and xylose.

Such reciprocal sugar interaction can lead to high selection pressure and thereby to physiological adaption as observed by the online monitoring system of this study. From a biochemical viewpoint, an increased expression of *ptsG* and *ptsF*, encoding for the glucose- and fructose-specific PTS transporters respectively, could lead to a better co-consumption of both sugars (Sasaki et al., 2011). With an increased abundance of PtsF mannose could bypass competition for PtsG with glucose. Also amino acid substitutions in PTS transporters can improve substrate uptake capacity, as recently reported for evolved fructose utilization by Krahn et al. (2021). Another potential target of genetic adaptations is transcriptional regulation (Engels et al., 2008; Gaigalat et al., 2007; Radek et al., 2017). Altered gene expression levels of, for example, sugar transporter genes have to be confirmed by RT-qPCR or global gene expression analyses. Changes in plasmid copy number (Prell et al., 2021) can be a further hypothetical explanation for the observed time-variable metabolic capacities under high selection pressure. Based on the recent work of Prell et al. (2021) plasmid copy numbers can be estimated to be in the approximate range of 100–130 for pEKEx3 and 10–20 for pVWEx1. From both a physiological (Sasaki et al., 2011) and process technological perspective (Sinner et al., 2019), mannose consumption can be regarded as the main bottleneck, causing sugar loss to the effluent and limiting biomass space time yield of the analyzed continuous process utilizing the mannose-rich by-product stream SSL. This is also reflected by the high sensitivities regarding mannose growth capacity on the measured process outputs. This high selection pressure towards mannose utilization leads to the observed steady increase of the mannose related parameter $\mu_{max\ S2}$.

To further analyze and clarify the biochemical basis of observed metabolic capacity changes, plasmid copy number determination, gene expression profiling and whole genome sequencing will be tackled in future work. In addition to that, the model structure can be potentially extended by intracellular resource allocation (Kremling et al., 2018) to describe the phenomenon of a reduced xylose uptake in favor of more cost-efficient substrate utilization pathways.

3.5 | Ensuring optimal operation under changing metabolic capacities

Online estimated states and parameters (Section 3.3) are essential for reliable process monitoring but can also be further used to predict optimal as well as critical operating conditions. In continuous cultivations the critical dilution rate represents the maximum dilution rate that can be applied before biomass washout occurs, and can thereby be regarded as the overall maximum metabolic conversion capacity of a chemostat.

Based on online adapted parameters the most probable current critical dilution rate can be obtained as shown for the second validation run (Data set 3) in Figure 7 (orange solid line). This capacity threshold is gradually increasing from 0.234 to 0.315 h^{-1} when dilution rate setpoints, and thereby selection pressure, are increased from app. 100 h process time onward. In contrast, critical dilution rate remains constant for a particle filter without parameter adaption (bluedashed line). During online monitoring of the biomass formation rate of the chemostat, this results in incorrectly low estimated specific growth rates (blue dotted line) in comparison to offline reference measurements (black solid line) when the process exceeds the static

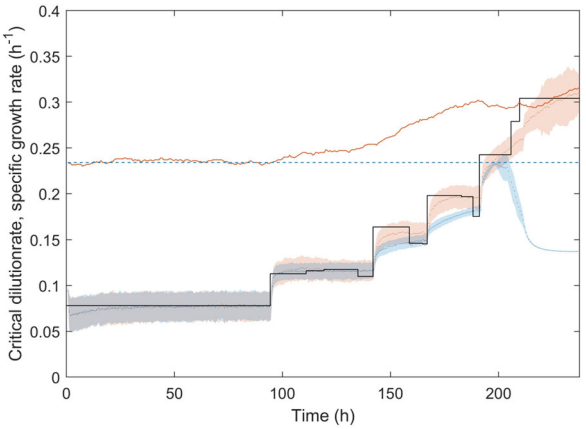

FIGURE 7 Online monitoring of specific growth rates and overall metabolic capacity (critical dilution rate) during a validation chemostat run with increasing dilution rate setpoints (Data set 3). Offline measured specific growth rate (black, solid line) and online monitored specific growth rate using particle filtering with constant metabolic capacity (blue, dotted line) or, respectively, with parallel state and parameter estimation (orange, dotted line). Shaded areas indicate 95% confidence intervals. Critical dilution rates are shown for constant (blue, dashed line) and online adapted metabolic capacity (orange, solid line)

capacity threshold. When a particle filter with parameter adaption is used instead, specific growth rates are monitored with satisfactory accuracy (orange dotted line). This underlines that the monitoring system considering long-term adaption effects can be successfully applied in operational regions exceeding the initially assumed capacity boundaries.

In addition, optimal operating points can be determined. In this study, high volumetric biomass productivity in combination with high sugar conversion efficiency (sugar loss in the effluent below 10%) were targeted. Based on multiobjective optimization, Pareto-optimal dilution rates for different process time points (Data set 3) were computed and displayed as circles within the phase diagrams in Figure 8. The first graph shows the relation between biomass productivity and conversion efficiency given in % sugar loss. The second and third graph display the two optimization criteria in function of the dilution rate setpoint. Due to adapted metabolic capacities, reflected in changing model parameters estimated by the particle filter, the system behavior of the process (solid lines) changes in course of the chemostat process. Selected optimal dilution rate setpoints with maximum biomass productivity satisfying the predefined sugar loss threshold are then selected (blue filled circles).

In function of the long-term adaption effects of the culture, washout boundary conditions shifted and the optimal dilution rate almost doubled from 0.11 h^{-1} at process startup to 0.20 h^{-1} after 235 h process time. Biomass space time yield substantially improved from 2.4 to 4.3 g L^{-1} h^{-1}. Also the functional relation between the two (competing) objectives changed. For instance, an increase of dilution rate during the initial process phase would only slightly increase

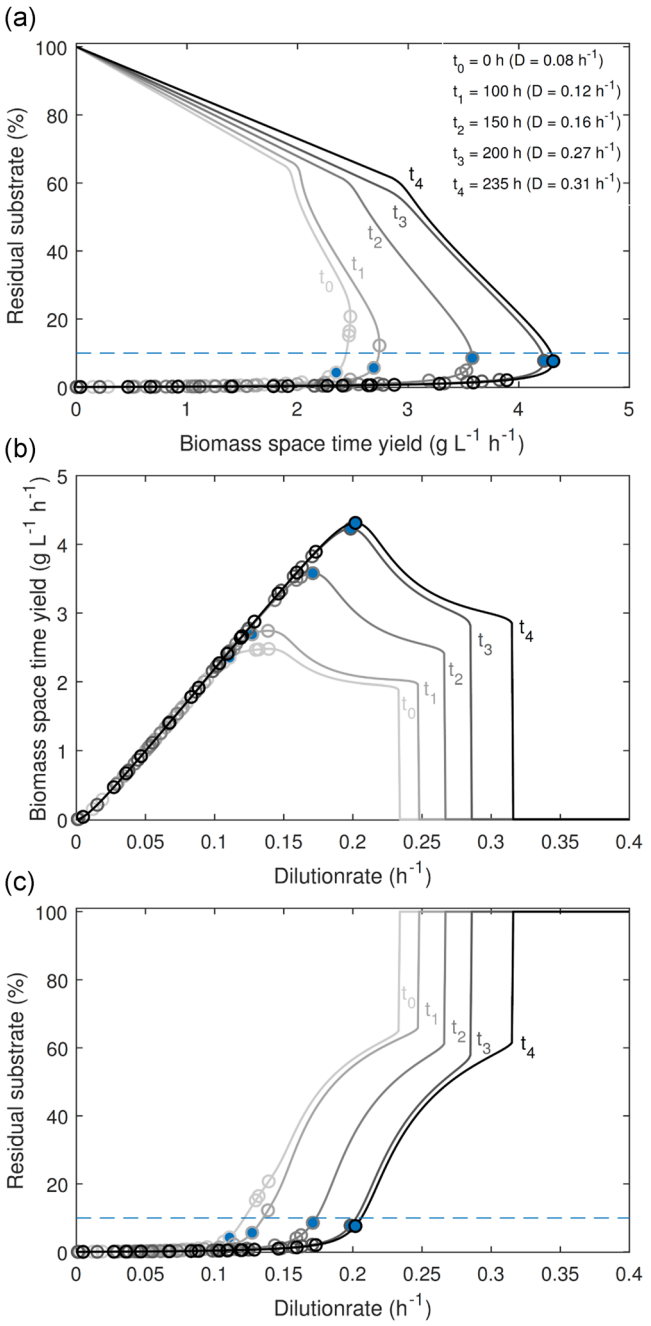

FIGURE 8 Maintenance of input-output relationships of a chemostat operated at increasing dilution rates (Data set 3, D_0 = 0.08 h^{-1} at t_0 = 0 h, D_1 = 0.12 h^{-1} at t_1 = 100 h, D_2 = 0.16 h^{-1} at t_2 = 150 h, D_3 = 0.27 h^{-1} at t_3 = 200 h, D_4 = 0.31 h^{-1} at t_1 = 235 h, see Figure 4) based on online estimated parameters (see Figure 6). Simulated steady state behavior is shown for all operational regions (solid lines) and for Pareto-optimal solutions (circles) maximizing biomass space time yield and minimizing substrate loss. Defining a maximum substrate loss threshold of 10% (dashed line), optimal setpoints are selected (blue filled circles). (a) Interdependence between biomass space time yield and residual substrate lost to the effluent. (b) Biomass space time yield in dependence of dilutionrate setpoint. (c) Substrate loss in dependence of dilutionrate setpoint

biomass productivity at the cost of high substrate loss (see grey circles at t_0 in Figure 8). In contrast, the adapted culture at later process phases shows a significantly reduced trade-off between biomass productivity and substrate loss (see also curvature changes in Figure 8a).

The presented time-dependent exploration of process behavior enables a re-evaluation of operational limits and optimal operating points and can thereby support human operator decision making. By combining feedback control algorithms with the developed online monitoring system, *C. glutamicum* chemostat processes utilizing SSL could be optimally controlled under consideration of time-variable metabolic capacities. In pharmaceutical production, the re-evaluation of process input–output relationships to provide assurance of product quality is termed as design space maintenance, as shown for simulated roller compaction and penicillin production processes by Bano et al. (2019). Similarly, this study shows how simultaneous state and parameter estimation can be used to re-evaluate the input–output relationship during running continuous bioprocesses also considering physiological adaptation effects.

4 | CONCLUSIONS

Within this study state estimation under changing metabolic capacities is presented and applied to continuous *C. glutamicum* cultivation processes utilizing the lignocellulosic by-product stream SSL, a complex sugar mixture mainly containing mannose, glucose and xylose. During prolonged chemostat processes with increasing dilution rates physiological adaption occurred, leading to high state estimation errors and wrong prediction of biomass washout under usage of static model parameters obtained from calibration data. To enable accurate monitoring under changing metabolic capacities a particle filter for simultaneous state and parameter estimation was established. Hereby, noninvasive off-gas analysis was used as online measurement and sugar utilization parameters were adapted during particle filtering. The results for a verification data set with increasing dilution rates show that integrating parametric variability enabled accurate estimation of biomass formation (RMSE of 1.4 g L^{-1}) and the utilization of carbon substrates (RMSE below 1.5 g L^{-1}), outperforming regular filtering assuming constant metabolic capacities. Analysis of the parameter trajectories and their sensitivities revealed that especially mannose consumption, being the main sugar in SSL, was improved over time. Only at dilution rates close to maximal metabolic capacities the selection pressure shifted towards the preferred glucose. Heterologously introduced and energetically suboptimal xylose consumption remained largely unchanged.

For practical applications of CSTR process engineering, quantitative information on the current metabolic capacities is of crucial importance. Having these available online, operational parameters such as dilution rate can be adjusted to ensure optimal efficiency of substrate utilization and volumetric productivity. As only noninvasive off-gas measurements are needed, the presented PAT system can be regarded as an add-on monitoring tool to retrofit existing biorefinery processes utilizing lignocellulosic by-product streams. Besides future investigation on the observed culture adaption by genomic and transcriptomic analysis, the developed state estimator needs to be employed for online feedback control. Thereby, model-based state and parameter estimation considering long-term adaption effects has the potential to further promote the usage of alternative feedstocks and to establish more efficient continuous cultivation processes.

ACKNOWLEDGEMENTS

This project has received funding from the Bio Based Industries Joint Undertaking under the European Union's Horizon 2020 research and innovation programme under grant agreement No 790507 (iFermenter), and from the COMET Center CHASE (project No 868615), which is funded within the framework of COMET (Competence Centers for Excellent Technologies) by BMVIT, BMDW, and the Federal Provinces of Upper Austria and Vienna. The COMET programme is run by the Austrian Research Promotion Agency (FFG). Further funding was provided by the German Ministry of Education and Research in the frame of the e:Bio initiative (contract No 555 031A302D), and the Novo Nordisk Fonden within the framework of the Fermentation-based Biomanufacturing Initiative (grant number NNF17SA0031362). The authors acknowledge TU Wien Bibliothek for financial support through its Open Access Funding Program.

AUTHOR CONTRIBUTIONS

Peter Sinner, Christoph Herwig, and Julian Kager conceived and designed the study. Oliver Goldbeck and Gerd M. Seibold performed strain design and construction. Peter Sinner, Marlene Stiegler, and Julian Kager performed the chemostat experiments. Peter Sinner analyzed the data and developed the software. Peter Sinner, Julian Kager, and Oliver Goldbeck wrote the manuscript. All authors reviewed, edited, and approved the final manuscript.

DATA AVAILABILITY STATEMENT

The data that support the findings of this study are available from the corresponding author upon reasonable request.

ORCID

Peter Sinner https://orcid.org/0000-0002-2838-0290
Oliver Goldbeck https://orcid.org/0000-0002-5708-8600
Gerd M. Seibold https://orcid.org/0000-0002-9823-8134
Christoph Herwig http://orcid.org/0000-0003-2314-1458
Julian Kager http://orcid.org/0000-0001-7274-6678

REFERENCES

Aehle, M., Kuprijanov, A., Schaepe, S., Simutis, R., & Lübbert, A. (2011). Simplified off-gas analyses in animal cell cultures for process monitoring and control purposes. *Biotechnology Letters*, *33*(11), 2103.

Ali, J. M., Hoang, N. H., Hussain, M. A., & Dochain, D. (2015). Review and classification of recent observers applied in chemical process systems. *Computers & Chemical Engineering*, *76*, 27–41.

Arensdorf, J. J., Loomis, A. K., DiGrazia, P. M., Monticello, D. J., & Pienkos, P. T. (2002). Chemostat approach for the directed evolution of biodesulfurization gain-of-function mutants. *Applied and Environmental Microbiology*, *68*(2), 691–698.

Badran, A. H., & Liu, D. R. (2015). In vivo continuous directed evolution. *Current Opinion in Chemical Biology*, *24*, 1–10.

Bano, G., Facco, P., Ierapetritou, M., Bezzo, F., & Barolo, M. (2019). Design space maintenance by online model adaptation in pharmaceutical manufacturing. *Computers & Chemical Engineering*, *127*, 254–271.

Bayen, T., & Mairet, F. (2017). Optimisation of strain selection in evolutionary continuous culture. *International Journal of Control*, *90*(12), 2748–2759.

Becker, J., Rohles, C. M., & Wittmann, C. (2018). Metabolically engineered Corynebacterium glutamicum for bio-based production of chemicals, fuels, materials, and healthcare products. *Metabolic Engineering*, *50*, 122–141.

Brun, R., Reichert, P., & Künsch, H. R. (2001). Practical identifiability analysis of large environmental simulation models. *Water Resources Research*, *37*(4), 1015–1030.

Brüsseler, C., Radek, A., Tenhaef, N., Krumbach, K., Noack, S., & Marienhagen, J. (2018). The myo-inositol/proton symporter IolT1 contributes to d-xylose uptake in Corynebacterium glutamicum. *Bioresource Technology*, *249*, 953–961.

Buschke, N., Becker, J., Schäfer, R., Kiefer, P., Biedendieck, R., & Wittmann, C. (2013). Systems metabolic engineering of xylose-utilizing Corynebacterium glutamicum for production of 1,5-diaminopentane. *Biotechnology Journal*, *8*(5), 557–570.

Buschke, N., Schäfer, R., Becker, J., & Wittmann, C. (2013). Metabolic engineering of industrial platform microorganisms for biorefinery applications - Optimization of substrate spectrum and process robustness by rational and evolutive strategies. *Bioresoure Technology*, *135*, 544–554. https://doi.org/10.1016/j.biortech.2012.11.047

Cabaneros Lopez, P., Udugama, I. A., Thomsen, S. T., Roslander, C., Junicke, H., Iglesias, M. M. & Gernaey, K. V. (2020a). Towards a digital twin: a hybrid data-driven and mechanistic digital shadow to forecast the evolution of lignocellulosic fermentation. *Biofuels, Bioproducts and Biorefining*. https://doi.org/10.1002/bbb.2108

Cabaneros Lopez, P., Udugama, I. A., Thomsen, S. T., Roslander, C., Junicke, H., Iglesias, M. M. & Gernaey, K. V. (2020b). Transforming data to information: A parallel hybrid model for real-time state estimation in lignocellulosic ethanol fermentation. *Biotechnology and Bioengineering*. https://doi.org/10.1002/bit.27586

Choi, J. W., Jeon, E. J., & Jeong, K. J. (2019). Recent advances in engineering *Corynebacterium glutamicum* for utilization of hemicellulosic biomass. *Current Opinion in Biotechnology*, *57*, 17–24.

Deb, K., Pratap, A., Agarwal, S., & Meyarivan, T. (2002). A fast and elitist multiobjective genetic algorithm: NSGA-II. *IEEE Transactions on Evolutionary Computation*, *6*(2), 182–197.

diè ne Benyahia, B., Campillo, F., Cherki, B. & rô me Harmand, J. (2012). Particle filtering for the chemostat. In *2012 20th Mediterranean Conference On Control & Automation (MED)* (pp. 364–371). https://doi.org/10.1109/MED.2012.6265665

d'Oelsnitz, S., & Ellington, A. (2018). Continuous directed evolution for strain and protein engineering. *Current Opinion in Biotechnology*, *53*, 158–163.

Engels, V., Lindner, S. N., & Wendisch, V. F. (2008). The global repressor SugR controls expression of genes of glycolysis and of the L-lactate dehydrogenase LdhA in Corynebacterium glutamicum. *Journal of Bacteriology*, *190*(24), 8033–8044.

Gagnon, M., Nagre, S., Wang, W., & Hiller, G. W. (2018). Shift to high-intensity, low-volume perfusion cell culture enabling a continuous, integrated bioprocess. *Biotechnology Progress*, *34*(6), 1472–1481.

Gaigalat, L., Schlüter, J.-P., Hartmann, M., Mormann, S., Tauch, A., Pühler, A., & Kalinowski, J. (2007). The DeoR-type transcriptional regulator SugR acts as a repressor for genes encoding the phosphoenolpyruvate:sugar phosphotransferase system (PTS) in Corynebacterium glutamicum. *BMC Molecular Biology*, *8*(1), 1–20.

Goffaux, G., & Vande Wouwer, A. (2005). Bioprocess state estimation: Some classical and less classical approaches. In T. Meurer, K. Graichen, & E. D. Gilles (Eds.), *Control and observer design for nonlinear finite and infinite dimensional systems* (pp. 111–128). Springer. https://doi.org/10.1007/11529798_8

Gold, D., Mohagheghi, A., Cooney, C. L., & Wang, D. I. (1981). Single-cell protein production from spent sulfite liquor utilizing cell-recycle and computer monitoring. *Biotechnology and Bioengineering*, *23*(9), 2105–2116. https://doi.org/10.1002/bit.260230914

Gordon, N. J., Salmond, D. J., & Smith, A. F. (1993). Novel approach to nonlinear/non-gaussian bayesian state estimation. In *IEE Proceedings F (radar and signal processing)* (Vol. *140*, pp. 107–113).

Graf, M., Haas, T., Teleki, A., Feith, A., Cerff, M., Wiechert, W., Nöh, K., Busche, T., Kalinowski, J., & Takors, R. (2020). Revisiting the growth modulon of *Corynebacterium glutamicum* under glucose limited chemostat conditions. *Frontiers in Bioengineering and Biotechnology 8*, 8.

Hemmerich, J., Moch, M., Jurischka, S., Wiechert, W., Freudl, R., & Oldiges, M. (2019). Combinatorial impact of Sec signal peptides from Bacillus subtilis and bioprocess conditions on heterologous cutinase secretion by *Corynebacterium glutamicum*. *Biotechnology and Bioengineering*, *116*(3), 644–655.

Herwig, C., & vonStockar, U. (2002). A small metabolic flux model to identify transient metabolic regulations in *Saccharomyces cerevisiae*. *Bioprocess and Biosystems Engineering*, *24*(6), 395–403.

Hoffmann, F. & Rinas, U. (2004). Stress induced by recombinant protein production in escherichia coli. In Physiological stress responses in bioprocesses. Advances in Biochemical Engineering (pp. 73–92). Springer.

Jansen, M. L., Diderich, J. A., Mashego, M., Hassane, A., de Winde, J. H., Daran-Lapujade, P., & Pronk, J. T. (2005). Prolonged selection in aerobic, glucose-limited chemostat cultures of *Saccharomyces cerevisiae* causes a partial loss of glycolytic capacity. *Microbiology*, *151*(5), 1657–1669.

Kazemi Seresht, A., Cruz, A. L., de Hulster, E., Hebly, M., Palmqvist, E. A., van Gulik, W., Daran, J.-M., Pronk, J., & Olsson, L. (2013). Long-term adaptation of *Saccharomyces cerevisiae* to the burden of recombinant insulin production. *Biotechnology and Bioengineering*, *110*(10), 2749–2763.

Keilhauer, C., Eggeling, L., & Sahm, H. (1993). Isoleucine synthesis in *Corynebacterium glutamicum*: Molecular analysis of the ilvB-ilvN-ilvC operon. *Journal of Bacteriology*, *175*(17), 5595–5603.

Kitagawa, G. (1998). A self-organizing state-space model. *Journal of the American Statistical Association*, 1203–1215.

Kittler, S., Kopp, J., Veelenturf, P. G., Spadiut, O., Delvigne, F., Herwig, C., & Slouka, C. (2020). The Lazarus *Escherichia coli* effect: Recovery of productivity on glycerol/lactose mixed feed in continuous biomanufacturing. *Frontiers in Bioengineering and Biotechnology*, *8*, 993.

Kopp, J., Slouka, C., Spadiut, O., & Herwig, C. (2019). The rocky road from fed-batch to continuous processing with *E. coli*. *Frontiers in Bioengineering and Biotechnology*, *7*, 328.

Koppram, R., Albers, E., & Olsson, L. (2012). Evolutionary engineering strategies to enhance tolerance of xylose utilizing recombinant yeast to inhibitors derived from spruce biomass. *Biotechnology for Biofuels*, *5*(1), 32.

Koprinkova-Hristova, P., & Patarinska, T. (2006). Neural network modelling of continuous microbial cultivation accounting for the memory effects. *International Journal of Systems Science*, *37*(5), 271–277.

Krahn, I., Bonder, D., Torregrosa, L., Stoppel, D., Krause, J. P., Rosenfeldt, N., Meiswinkel, T. M., Seibold, G. M., Wendisch, V. F., &

Lindner, S. N. (2021). Evolving a new efficient mode of fructose utilization for improved bioproduction in Corynebacterium glutamicum. Frontiers in Biotechnology and Bioengineering.

Kremling, A., Geiselmann, J., Ropers, D., & de Jong, H. (2018). An ensemble of mathematical models showing diauxic growth behaviour. *BMC Systems Biology*, *12*(1), 1–16.

Kroll, P., Hofer, A., Stelzer, I. V., & Herwig, C. (2017). Workflow to set up substantial target-oriented mechanistic process models in bioprocess engineering. *Process Biochemistry*, *62*, 24–36.

Ladakis, D., Michailidi, K., Vlysidis, A., Koutinas, A., & Kookos, I. K. (2018). Valorization of spent sulphite liquor for succinic acid production via continuous fermentation system. *Biochemical Engineering Journal*, *137*, 262–272.

Lawford, H. G., & Rousseau, J. D. (1993). Production of ethanol from pulp mill hardwood and softwood spent sulfite liquors by genetically engineered *E. coli*. *Applied Biochemistry and Biotechnology*, *39*(1), 667–685.

Lindner, S. N., Seibold, G. M., Henrich, A., Krämer, R., & Wendisch, V. F. (2011). Phosphotransferase system-independent glucose utilization in *Corynebacterium glutamicum* by inositol permeases and glucokinases. *Applied and Environmental Microbiology*, *77*(11), 3571–3581.

Mandenius, C. F. (1988). Controlling fermentation of lignocellulose hydrolysates in a continuous hollow-fiber reactor using biosensors. *Biotechnology and Bioengineering*, *32*(2), 123–129.

Meiswinkel, T. M., Gopinath, V., Lindner, S. N., Nampoothiri, K. M., & Wendisch, V. F. (2013). Accelerated pentose utilization by Corynebacterium glutamicum for accelerated production of lysine, glutamate, ornithine and putrescine. *Microbial Biotechnology*, *6*(2), 131–140.

Minkevich, I., & Eroshin, V. (1973). Productivity and heat generation of fermentation under oxygen limitation. *Folia Microbiologica*, *18*(5), 376–385.

Narayanan, H., Behle, L., Luna, M. F., Sokolov, M., Guillén-Gosálbez, G., Morbidelli, M., & Butté, A. (2020). Hybrid-ekf: Hybrid model coupled with extended Kalman filter for real-time monitoring and control of mammalian cell culture. *Biotechnology and Bioengineering*, *117*(9), 2703–2714.

Neubauer, P., Lin, H., & Mathiszik, B. (2003). Metabolic load of recombinant protein production: Inhibition of cellular capacities for glucose uptake and respiration after induction of a heterologous gene in *Escherichia coli*. *Biotechnology and Bioengineering*, *83*(1), 53–64.

Patarinska, T., Dochain, D., Agathos, S. N., & Ganovski, L. (2000). Modelling of continuous microbial cultivation taking into account the memory effects. *Bioprocess Engineering*, *22*(6), 517–527.

Patarinska, T., & Popova, S. (2003). Online biomass and specific growth rate estimation aimed to control of a chemostat microbial cultivation accounting for the memory effects. *Systems Analysis Modelling Simulation*, *43*(6), 693–720.

Prell, C., Busche, T., Rückert, C., Nolte, L., Brandenbusch, C., & Wendisch, V. F. (2021). Adaptive laboratory evolution accelerated glutarate production by *Corynebacterium glutamicum*. *Microbial Cell Factories*, *20*(1), 1–20.

Radek, A., Tenhaef, N., Müller, M. F., Brüsseler, C., Wiechert, W., Marienhagen, J., Polen, T., & Noack, S. (2017). Miniaturized and automated adaptive laboratory evolution: Evolving *Corynebacterium glutamicum* towards an improved D-xylose utilization. *Bioresource Technology*, *245*, 1377–1385.

Sahm, H., & Bringer-Meyer, S. (1987). Continuous ethanol production by *Zymomonas mobilis* on an industrial scale. *Acta Biotechnologica*, *7*(4), 307–313.

Sasaki, M., Teramoto, H., Inui, M., & Yukawa, H. (2011). Identification of mannose uptake and catabolism genes in *Corynebacterium glutamicum* and genetic engineering for simultaneous utilization of mannose and glucose. *Applied Microbiology and Biotechnology*, *89*(6), 1905–1916.

Sato, T. K., Tremaine, M., Parreiras, L. S., Hebert, A. S., Myers, K. S., Higbee, A. J., Sardi, M., McIlwain, S. J., Ong, I. M., Breuer, R. J., AvanasiNarasimhan, R., McGee, M. A., Dickinson, Q., LaReau, A., Xie, D., Tian, M., Reed, J. L., Zhang, Y., Coon, J. J., … Landick, R. (2016). Directed evolution reveals unexpected epistatic interactions that alter metabolic regulation and enable anaerobic xylose use by Saccharomyces cerevisiae. *PLOS Genetics*, *12*(10), e1006372.

Schuller, A., Cserjan-Puschmann, M., Köppl, C., Grabherr, R., Wagenknecht, M., Schiavinato, M., Dohm, J. C., Himmelbauer, H., & Striedner, G. (2020). Adaptive evolution in producing microtiter cultivations generates genetically stable Escherichia coli production hosts for continuous bioprocessing. *Biotechnology Journal*, 2000376.

Schwentner, A., Neugebauer, H., Weinmann, S., Santos, H., & Eikmanns, B. J. (2021). Exploring the potential of Corynebacterium glutamicum to produce the compatible solute mannosylglycerate. *Frontiers in Bioengineering and Biotechnology*, *9*, 811.

Simon, D. (2006). *Optimal state estimation: Kalman, H infinity, and nonlinear approaches*. John Wiley & Sons.

Sinner, P., Kager, J., Daume, S., & Herwig, C. (2019). Model-based analysis and optimisation of a continuous Corynebacterium glutamicum bioprocess utilizing lignocellulosic waste. *IFAC-PapersOnLine*, *52*(26), 181–186.

Sinner, P., Stiegler, M., Herwig, C., & Kager, J. (2021). Noninvasive online monitoring of *Corynebacterium glutamicum* fed-batch bioprocesses subject to spent sulfite liquor raw material uncertainty. *Bioresource Technology*, 321.

Sonnleitner, B., & Hahnemann, U. (1994). Dynamics of the respiratory bottleneck of *Saccharomyces cerevisiae*. *Journal of Biotechnology*, *38*(1), 63–79.

Spérandio, M., & Paul, E. (1997). Determination of carbon dioxide evolution rate using on-line gas analysis during dynamic biodegradation experiments. *Biotechnology and Bioengineering*, *53*(3), 243–252.

Stelzer, I. V., Kager, J. & Herwig, C. (2017). Comparison of particle filter and extended kalman filter algorithms for monitoring of bioprocesses. In A. Espuña, M. Graells, & L. Puigjaner (Eds.), 27th European symposium on computer aided process engineering (Vol. 40, pp. 1483–1488). Elsevier. https://doi.org/10.1016/B978-0-444-63965-3.50249-X

Uhde, A., Youn, J.-W., Maeda, T., Clermont, L., Matano, C., Krämer, R., Wendisch, V. F., Seibold, G. M., & Marin, K. (2013). Glucosamine as carbon source for amino acid-producing *Corynebacterium glutamicum*. *Applied Microbiology and Biotechnology*, *97*(4), 1679–1687.

Ulonska, S., Kroll, P., Fricke, J., Clemens, C., Voges, R., Müller, M. M., & Herwig, C. (2018). Workflow for target-oriented parametrization of an enhanced mechanistic cell culture model. *Biotechnology Journal*, *13*(4), 1700395.

Vees, C. A., Veiter, L., Sax, F., Herwig, C., & Pflügl, S. (2020). A robust flow cytometry-based biomass monitoring tool enables rapid at-line characterization of *S. cerevisiae* physiology during continuous bioprocessing of spent sulfite liquor. *Analytical and Bioanalytical Chemistry*, 1–13.

Wenger, J. W., Piotrowski, J., Nagarajan, S., Chiotti, K., Sherlock, G., & Rosenzweig, F. (2011). Hunger artists: Yeast adapted to carbon limitation show trade-offs under carbon sufficiency. *PLOS Genetics*, *7*(8), e1002202.

Wick, L. M., Weilenmann, H., & Egli, T. (2002). The apparent clock-like evolution of *Escherichia coli* in glucose-limited chemostats is

reproducible at large but not at small population sizes and can be explained with Monod kinetics. *Microbiology*, *148*(9), 2889–2902.

Wortel, M. T., Bosdriesz, E., Teusink, B., & Bruggeman, F. J. (2016). Evolutionary pressures on microbial metabolic strategies in the chemostat. *Scientific Reports*, *6*, 29503.

Wright, N. R., Wulff, T., Palmqvist, E. A., Jørgensen, T. R., Workman, C. T., Sonnenschein, N., Rønnest, N. P., & Herrgård, M. J. (2020). Fluctuations in glucose availability prevent global proteome changes and physiological transition during prolonged chemostat cultivations of *Saccharomyces cerevisiae*. *Biotechnology and Bioengineering*, *117*(7), 2074–2088.

Yoon, H., Klinzing, G., & Blanch, H. (1977). Competition for mixed substrates by microbial populations. *Biotechnology and Bioengineering*, *19*(8), 1193–1210.

SUPPORTING INFORMATION

Additional supporting information may be found in the online version of the article at the publisher's website.

How to cite this article: Sinner, P., Stiegler, M., Goldbeck, O., Seibold, G. M., Herwig, C., & Kager, J. (2022). Online estimation of changing metabolic capacities in continuous *Corynebacterium glutamicum* cultivations growing on a complex sugar mixture. *Biotechnology and Bioengineering*, 119, 575–590. https://doi.org/10.1002/bit.28001